Selective recovery and efficient separation of lithium, rubidium, and cesium from lepidolite ores

Yubo Liu [a,b], Baozhong Ma [a,b,c,*], Yingwei Lv [a,b], Chengyan Wang [a,b,c,*], Yongqiang Chen [a,b,c]

[a] State Key Laboratory of Advanced Metallurgy, University of Science and Technology Beijing, Beijing 100083, China
[b] School of Metallurgical and Ecological Engineering, University of Science and Technology Beijing, Beijing 100083, China
[c] Beijing Key Laboratory of Green Recovery and Extraction of Rare and Precious Metals, University of Science and Technology Beijing, Beijing 100083, China

ARTICLE INFO

ABSTRACT

Sulfation and decomposition were proposed to selectively recover lithium, rubidium, and cesium from lepidolite ore. The purpose was to solve the problems of high acid consumption and the difficulty of separating lithium and aluminum in the sulfuric acid method. First, the theoretical feasibility of the process was verified by thermodynamic calculations. The optimal parameters were determined according to the theoretical and experimental results. The extraction rates of lithium, rubidium, and cesium were 90.5%, 91.2%, and 89.4%, respectively, whereas those of aluminum and iron were only 0.08% and 0.02%, respectively. The selective extraction of lithium, rubidium, and cesium was realized, and 90.4% of sulfuric acid could be recycled during the process. Subsequently, the mechanism was discussed by XRD and SEM-EDS analysis. The first-step roasting was the sulfation process of lepidolite, and the second-step roasting was the decomposition process of partial sulfates. The separation of alkali elements and impurity elements could be realized by simple deionized water leaching. The production of Li_2CO_3 and single-alkali sulfates (K_2SO_4, Rb_2SO_4, and Cs_2SO_4) were obtained through the efficient separation methods of carbonization precipitation and solvent extraction. This process achieved the selective recovery and efficient separation of lithium, rubidium, and cesium from lepidolite ores. At the same time, the recycling of sulfuric acid was realized; it greatly reduced the amount of reagents, such as acid and alkali. It is an efficient, clean, and sustainable process for the utilization of lepidolite ores.

1. Introduction

Lithium is the most significant new energy metal in the 21st century [1]. According to statistics, the global consumption of lithium has more than doubled from 24.5 kt in 2010 to 56.0 kt in 2020 in the past 10 years [2]. Among them, the consumption in the field of batteries has grown particularly rapidly [3,4], and the proportion of which has increased from 23% in 2010 [5] to 71% in 2020 [6]. In addition, the 2019 Nobel Prize in Chemistry was awarded to Goodenough and two other experts in the field of lithium batteries, thereby showing the importance of lithium in the modern energy industry [7]. Considering that many countries still rely on fossil energy sources, steady increase in the demand for lithium in the global market is foreseeable for a long period of time in the future [8,9]. Rubidium and cesium are mainly used in academic research and technological development [10]. In recent years, they have gradually emerged in the fields of aerospace [11], quantum computing [12], biomedicine [13], and quantum heat engines [14] due to their excellent

chemical and optoelectronic properties [15]. With the rapid development of science and technology today, lithium, rubidium, and cesium play increasingly significant roles in various emerging fields [16]. Therefore, the extraction and recovery of lithium, rubidium, and cesium have social and economic importance. Lepidolite, with the chemical formula of $K[Li_{2-x}Al_{1+x}(Al_{2x}Si_{4-2x}O_{10})(F,OH)_2]$ (x = 0–0.5), is a common lithium-bearing silicate mineral with glassy luster [17,18]. It is mainly distributed in granite pegmatite and is usually accompanied by spodumene and muscovite [19]. The chemical composition of lepidolite ores is generally 3% −7.7% Li_2O, 5% −10% K_2O, 22% −29% Al_2O_3, and 47% −60% SiO_2 [20]. Part of the potassium could be replaced by high-value rubidium and cesium in the form of isomorphism [21], and part of the aluminum could be replaced by iron and manganese.

At present, the main methods for treating lepidolite ores include the sulfate roasting method [22–24], chlorination roasting method [25–27], thermal activation method [28], hydrofluoric acid method [29–31], and alkali autoclaving method [32,33]. Among them, the roasting methods

---

have the problem of energy consumption, which requires treatment at relatively high temperatures (850 °C–1300 °C) [22,26,28]. The hydrofluoric acid method needs to introduce a large amount of fluoride ions (HF dosage, approximately 200%) [29], not only increasing the difficulty of subsequent processes, but also causing the possibility of environmental pollution. The alkali autoclaving method has strict requirements for high-pressure equipment and a large consumption of alkali (600 g/L NaOH, L/S = 7:1) [33]. Thus, obtaining economic benefits in actual production is difficult. Recently, the treatment of lepidolite ores by the sulfuric acid method has been gradually observed by researchers. Vieceli et al. [34,35] initially ground the lepidolite ores to $d_{90} = 32.95$ μm by mechanical activation. Then, the lepidolite ores were baked with 0.96 g/g ores of concentrated sulfuric acid (98%) at 130 °C for 15 min, and a lithium extraction rate of over 90% was eventually obtained after leaching. Liu et al. [36] used 2.5 mL/g ores of dilute sulfuric acid (50%) to leach lepidolite ores (–100 μm) continuously at 138 °C for 10 h in a three-necked flask with a condenser. The recovery rate of lithium reached 94.8%. Zhang et al. [37] digested lepidolite ores at 200 °C for 4 h, and the sulfuric acid (85%) dosage was 1.7 g/g ores. The extraction of lithium, rubidium, and cesium at 85 °C was 97%, 96%, and 95%, respectively.

The sulfuric acid method could effectively extract valuable metals from lepidolite ores under relatively simple and mild conditions. However, the problem of high consumption of sulfuric acid (more than 100%) also existed, and a large amount of alkali (CaO or NaOH) was required to neutralize the residual acid in the subsequent process. More importantly, part of the aluminum and iron (approximately 50%) in lepidolite ores was leached during the leaching process of the sulfuric acid method. The preliminary exploratory experiments of our research group found that considerable lithium in leaching liquor was lost during the neutralization of the residual acid and the removal of aluminum and iron. The lithium contained in the iron–aluminum slags could not be washed away by deionized water, indicating that it was not caused by simple entrainment. Thus far, few reports have focused on these details. The existing studies on the treatment of lepidolite ores by the sulfuric acid method are mainly focused on the leaching process, and the subsequent process of separation and purification has not been systematically studied. At present, no good solution is found to solve the generation problem of lithium aluminate and lithium ferrite, which will be stated in the thermodynamic analysis section. Therefore, avoiding the leaching of aluminum and iron from the source is the most effective solution to avoid the loss of lithium.

A two-step sulfuric acid roasting method was proposed; it can selectively recover lithium, rubidium, and cesium from lepidolite ores without leaching iron or aluminum. (1) The first-step roasting: sulfation of lepidolite ores. (2) The second-step roasting: decomposition of partial sulfates. (3) Recycling of sulfuric acid. (4) Separation of rubidium and cesium. (5) Precipitation of lithium. The effects of various parameters on the extractions of each element during two-step sulfuric acid roasting were systematically studied. The feasibility of recycling sulfuric acid was discussed. XRD and SEM-EDS were used to analyze the reaction mechanism during the roasting process. Finally, the separation and purification of lithium, rubidium, and cesium in leach solution were studied by solvent extraction and carbonization precipitation, respectively.

2. Materials and methods

2.1. Materials

The lepidolite ores used in this process were obtained by flotation from the spodumene tailings and pretreated by grinding and screening to − 74 μm. After evenly mixing the ground lepidolite ore powders, the chemical components were detected, as shown in Table 1. It demonstrates that the content of lithium in lepidolite ores used in this process was relatively lower than that commonly recognized in lepidolite ores, whereas the content of rubidium was higher. Combined with the results of XRD analysis (Fig. 1), the characteristic peaks of muscovite (PDF#86-1385) were clearly found in addition to lepidolite (PDF#42-1399). The presence of lithium-free minerals led to a decrease in the content of lithium. Meanwhile, substantial potassium in muscovite could be replaced by rubidium and cesium in the form of isomorphism, which explained the increase in the content of rubidium. In addition, all chemicals used in the process were AR grade.

2.2. Procedures

The lepidolite ore powders (50 g) were evenly mixed with concentrated sulfuric acid (70 g) and deionized water (15 mL) in a porcelain crucible. Then, they were transferred to a muffle furnace (SX2-10-13, Tianjin Zhonghuan Electric Furnace, China) for the roasting process. The first-step (S1) started at 25 °C and rose to 300 °C, which was the destruction process of the lepidolite structure. The second-step (S2) was followed immediately to the predetermined temperature at a speed of 20 °C/min. The entire process was carried out in the furnace, and the crucible was taken out when cooled to room temperature. The roasting slags were leached directly with deionized water at the conditions of 2:1 mL/g, 80 °C and 2 h without further grinding. The solvent extraction of rubidium and cesium was performed in a separation funnel. CO_2 was introduced into the raffinate at room temperature to reduce the pH of the solution to 7–8, and then evaporated and crystallized to obtain the lithium precipitation product. The flowsheet for the selective recovery process of lithium, rubidium, and cesium from lepidolite ores is shown in Fig. 2.

2.3. Methods and characterizations

The extraction rates of components in lepidolite ores can be calculated by Eq. (1).
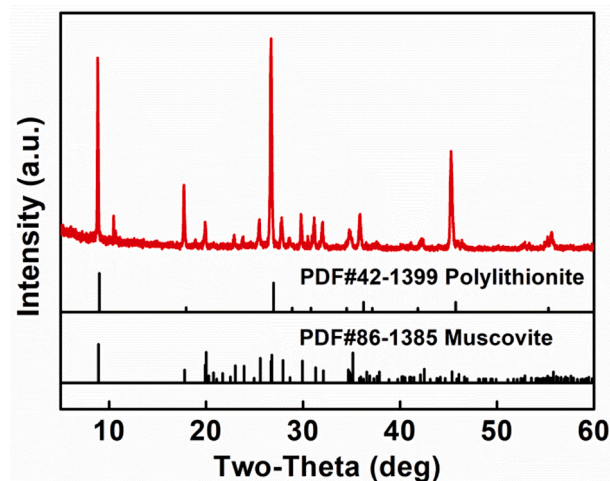
Fig. 1. XRD analysis of the lepidolite ores.

Table 1
The chemical components of the ground lepidolite ores powders (wt. %).

Li	Rb	Cs	Al	Fe	K	Mn	Mg	F	SiO$_2$
0.92	1.40	0.10	13.26	5.65	6.74	1.01	0.50	4.68	48.25
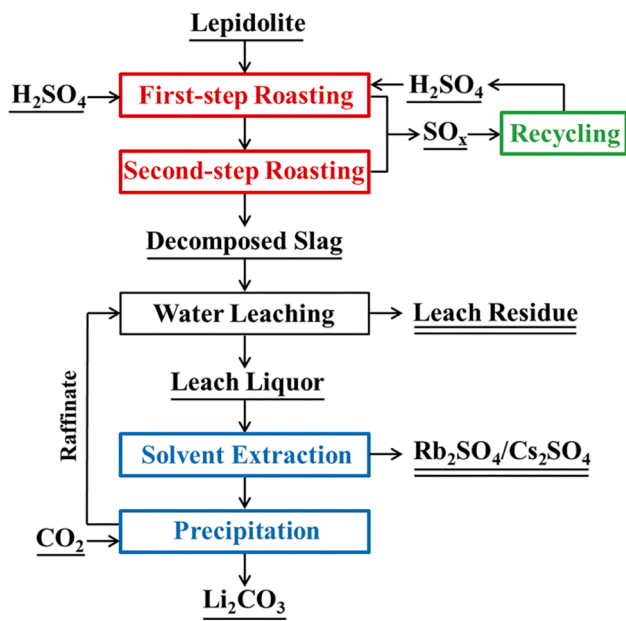
Fig. 2. Flowsheet for the selective recovery and efficient separation process of lithium, rubidium, and cesium from lepidolite ores.

$$\eta_i = \left(1 - \frac{m_r \times \omega_{r,i}}{m_0 \times \omega_i}\right) \times 100\% \tag{1}$$

where m_0 and m_r denote the mass of lepidolite ores and leaching residues, respectively, ω_i and $\omega_{r,i}$ denote the wt.% of component "i" in them.

The recovery of sulfur can be calculated by **Eq. (2)**.

$$\eta_S = \left(1 - \frac{V_l \times [S]_l}{V_0 \times [S]_0}\right) \times 100\% \tag{2}$$

where V_0 and V_l denote the volume of sulfuric acid and leaching liquor, respectively, $[S]_0$ and $[S]_l$ denote the concentrations of SO_4^{2-} in them.

The separation factor of Cs/Rb and Rb/K can be calculated by **Eqs. (3-1 and 3-2)**.

$$\beta_{Cs/Rb} = \frac{[Cs]_O}{[Cs]_A} \bigg/ \frac{[Rb]_O}{[Rb]_A} \tag{3-1}$$

$$\beta_{Rb/K} = \frac{[Rb]_O}{[Rb]_A} \bigg/ \frac{[K]_O}{[K]_A} \tag{3-2}$$

where $[K]_O$, $[Rb]_O$ and $[Cs]_O$ denote the concentrations of K, Rb and Cs in the organic phase, respectively, $[K]_A$, $[Rb]_A$ and $[Cs]_A$ denote the concentrations in the aqueous phase.

The contents of Li, Rb, and Cs were analyzed by AAS (Z-2000, Hitachi, Japan). The contents of Al and Fe in this study were carried out by ICP-OES (Optima 7000 DV, Perkin Elmer Instruments, U.S.). Other elements in the lepidolite ores were determined by XRF (XRF-1800, Shimadzu, Japan). The concentration of SO_4^{2-} in the leaching liquor was measured by IC (ICS-1100, Dionex, U.S.). The phase composition of raw ores, calcine, and leaching residue was performed by XRD (Ultima IV, Rigaku, Japan). The micromorphology and element distribution of the solid phase at each stage of the process were characterized by SEM-EDS (MLA250, FEI, U.S.).

3. Results and discussion

3.1. Thermodynamic analysis

3.1.1. Generation of lithium aluminate and lithium ferrite

The process of impurity removal in the leaching solution of sulfuric acid method was simulated. The XRD analysis of the impurity-removing slags is shown in Fig. 3(a). The co-precipitation reaction occurred with lithium and aluminum to generate $LiAl_2(OH)_7 \cdot 2H_2O$ during the process of aluminum removal. The lithium contained in the slags could not be washed away by deionized water, indicating that it was not caused by simple entrainment. The structure was relatively stable and might be the precursor of lithium aluminate [38,39]. The E-pH diagram (Fig. 3(b)) shows that the stable phase of lithium ferrite may be formed in the leaching liquor containing lithium, aluminum, and iron when the pH value reaches 0.75. Then, the stable phase of lithium aluminate or lithium ferrite must be formed at the pH above 3.51, which explains the loss of lithium during the process of impurity removal. On this basis, preventing the leaching of aluminum and iron from the source and realizing the selective extraction of lithium, rubidium, and cesium is the most effective scheme.

3.1.2. Thermodynamic modeling of the process

Thermodynamic modeling of the reaction of lepidolite ores with sulfuric acid from 25 °C to 1000 °C was calculated by HSC Chemistry 6.0. The thermodynamic data of lepidolite ores were not included in the database; thus, the mixture of Li_2O, K_2O, Rb_2O, Al_2O_3, and FeO corresponding to the content of raw ores was used. Silicon did not participate in the reaction during the entire process, the content of cesium was extremely low and the properties were similar to rubidium; thus, neither of them was included in the calculation. The calculated thermodynamic modeling is shown in Fig. 4(a). The results were classified by components to facilitate observation and analysis. Fig. 4(b) shows the phase changes of the potassium, aluminum, and sulfur components during the entire process. Fig. 4(c) depicts the components of rubidium and a phase of potassium not shown in Fig. 4(b). Fig. 4(d) describes the changes in iron components.

The sulfates were generated at the beginning of the calculated modeling due to the substitution of simple oxides for complex lepidolite ores. The thermodynamic modeling (Fig. 4(a)) clearly shows that the content of Li_2SO_4 remained unchanged throughout the process, and no other lithium phase was produced, indicating that Li_2SO_4 was extremely stable during the roasting process without any reaction. Fig. 4(b) shows that potassium mainly presented as the phase of $KAl(SO_4)_2 \cdot 3H_2O$ associated with a small amount of $KAl(SO_4)_2 \cdot 12H_2O$ at the beginning of the modeling. When the temperature reached 200 °C, they were completely dehydrated and converted into $KAl(SO_4)_2$ (**Eqs. (4,5)**). Then, it began to decompose into K_2SO_4, Al_2O_3, and SO_3 at a temperature of nearly 650 °C (**Eq. (6)**). The decomposition of $Al_2(SO_4)_3$ began at nearly 400 °C and converted into Al_2O_3 (**Eq. (7)**). Fig. 4(c) depicts that the rubidium phase was dehydrated from $RbAl(SO_4)_2 \cdot 12H_2O$ to $RbAl(SO_4)_2$ at approximately 160 °C (**Eq. (8)**). Subsequently, it also decomposed at nearly 650 °C, gradually transforming into Rb_2SO_4 (**Eq. (9)**). Fig. 4(d) demonstrates that $FeSO_4$ begins to oxidize and decompose into $Fe_2(SO_4)_3$, Fe_2O_3, and SO_2 at a temperature of nearly 300 °C (**Eq. (10)**). The content of $Fe_2(SO_4)_3$ reached a maximum at approximately 620 °C, and it also gradually decomposed into Fe_2O_3 (**Eq. (11)**).

Consequently, the alum products generated during sulfation were initially dehydrated at approximately 200 °C. Subsequently, the temperature rose to 300 °C to start the decomposition of $Al_2(SO_4)_3$ and the oxidation and decomposition of $FeSO_4$. Finally, the decomposition of $KAl(SO_4)_2$ and $RbAl(SO_4)_2$ occurred at approximately 650 °C. The ultimate products were soluble Li_2SO_4, K_2SO_4, and Rb_2SO_4 in water and insoluble Al_2O_3, Fe_2O_3, as well as gases SO_3 and SO_2. The analysis shows that this process can realize the selective extraction of lithium, rubidium, and cesium without leaching iron or aluminum from the perspective of thermodynamics.

$$KAl(SO_4)_2 \cdot 3H_2O(s) \rightarrow KAl(SO_4)_2(s) + 3H_2O(g) \tag{4}$$

$$KAl(SO_4)_2 \cdot 12H_2O(s) \rightarrow KAl(SO_4)_2(s) + 12H_2O(g) \tag{5}$$
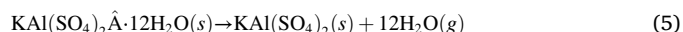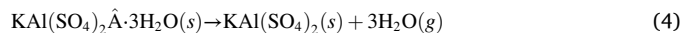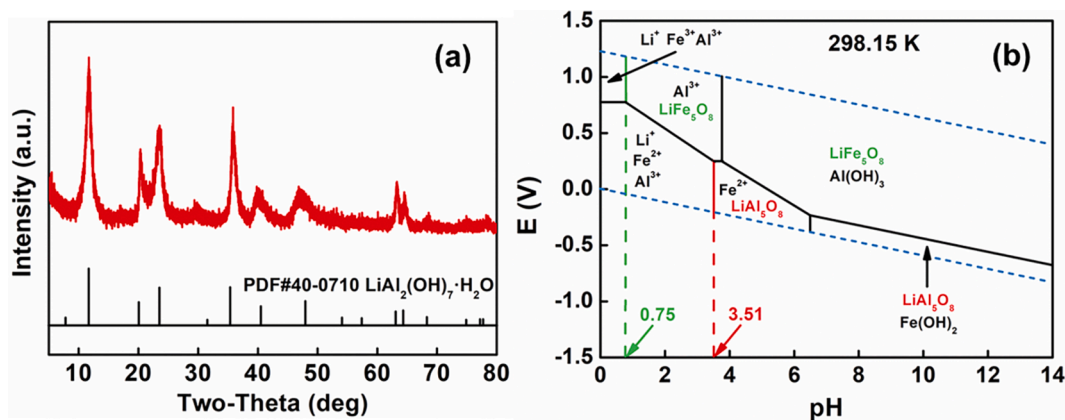
Fig. 3. (a) XRD analysis of the impurity-removing slags; (b) E-pH diagrams for the solution containing Li, Al, and Fe at 298.15 K.
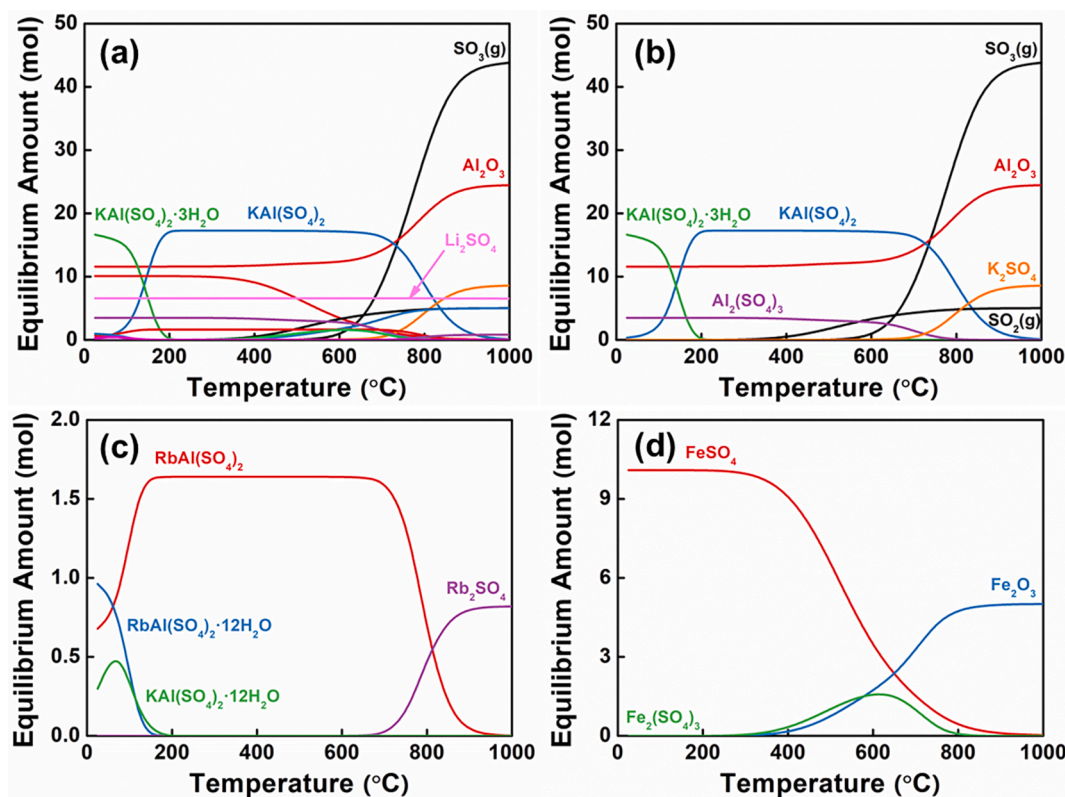
Fig. 4. (a) Thermodynamic modeling and the phase changes of components (b) K, Al, S, (c) Rb, and (d) Fe, individually.

$$2KAl(SO_4)_2(s) \rightarrow K_2SO_4(s) + Al_2O_3(s) + 3SO_3(g) \tag{6}$$

$$Al_2(SO_4)_3(s) \rightarrow Al_2O_3(s) + 3SO_3(g) \tag{7}$$

$$RbAl(SO_4)_2 \cdot 12H_2O(s) \rightarrow RbAl(SO_4)_2(s) + 12H_2O(g) \tag{8}$$

$$2RbAl(SO_4)_2(s) \rightarrow Rb_2SO_4(s) + Al_2O_3(s) + 3SO_3(g) \tag{9}$$

$$FeSO_4(s) \rightarrow Fe_2(SO_4)_3(s) + 2Fe_2O_3(s) + 3SO_2(g) \tag{10}$$

$$Fe_2(SO_4)_3(s) \rightarrow Fe_2O_3(s) + 3SO_3(g) \tag{11}$$
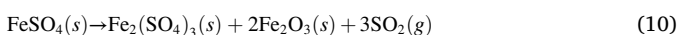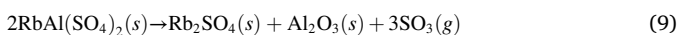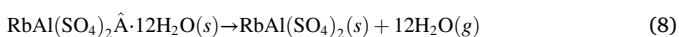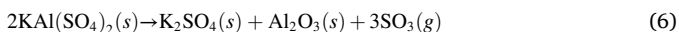
3.2. Sulfation process

Roasting S1 was the sulfation between lepidolite ores and sulfuric acid. The specific parameters of this reaction that would not be discussed

have been studied in detail in many articles [34–37]. The sulfation process adopted a slow and continuous heating process to achieve the continuity of the two-step roasting. The unstudied factor that affected this period was the heating time from 25 °C to 300 °C. After roasting S1, the sample was immediately obtained for leaching. The extraction rates of each component were calculated to study the effect of heating time, as shown in Fig. 5(a). This finding indicated that the extraction rate of Li was lower than 50% at a heating time of 0.5 h, and the rates of Rb and Cs were even lower than 30%. With the extension of heating time, the extraction rates of Li, Rb, and Cs all increased greatly. The plateaus were reached under the condition of 5 h, and the extraction rates of Li, Rb, and Cs were maintained at approximately 90.2%, 91.5%, and 88.2%, respectively. Meanwhile, the extraction of Al also increased slightly (from 37.5% to 60.3%) with longer heating times and trended toward a continuous increase after 6 h. Aluminum was the main element of the structure skeleton of lepidolite ores. The reason for the increasing Al
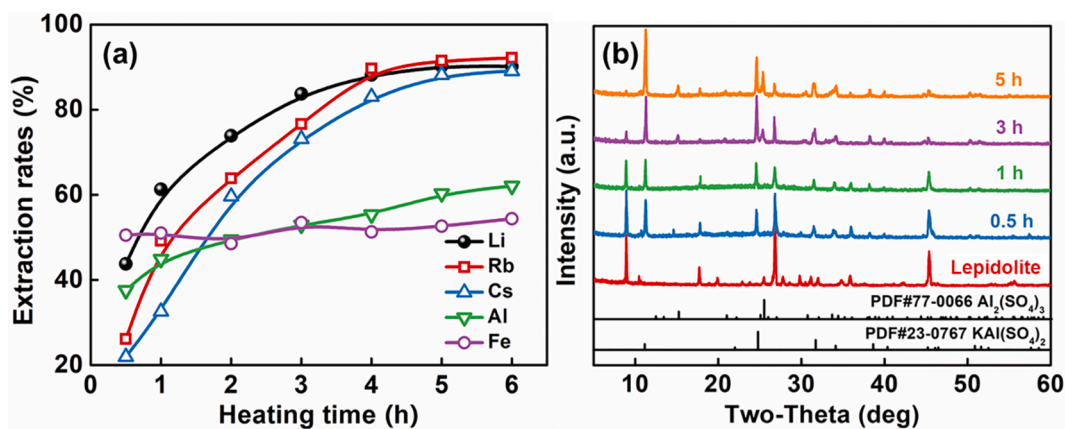
Fig. 5. Effect of heating time on (a) the extraction rates of Li, Rb, Cs, Al, and Fe; (b) XRD patterns of the roasting slags during roasting S1.

extraction was the continuous destruction of mineral structures. The extraction of Fe was almost stable at approximately 50% throughout the process, which was probably because most Fe is not present in the lepidolite ores but in other more stable iron-bearing minerals, such as amphibole. According to the XRD analysis of the roasting S1 slags with different heating times (Fig. 5(b)), strong diffraction peaks of lepidolite ores could still be clearly observed at 0.5 h and 1 h. The sulfation of lepidolite ores was relatively lower at this time, which also confirmed the lower extraction rates of Li, Rb, and Cs in Fig. 5(a). When the heating time reached 3 h, the intensity of the lepidolite peaks in the slags became much weaker, and they almost disappeared at the heating time of 5 h, indicating that the structure of lepidolite ores had been thoroughly demolished. On the contrary, the diffraction peaks of newly formed KAl(SO$_4$)$_2$ and Al$_2$(SO$_4$)$_3$ became increasingly stronger. To ensure the extraction of Li, Rb, and Cs and facilitate the subsequent separation of Al and Fe, roasting S1 pursued the lowest extraction of Al and Fe under the premise of the highest extraction of Li, Rb, and Cs. Hence, 5 h was considered the best heating time for roasting S1.

3.3. Decomposition process

3.3.1. Effect of roasting temperature

In the thermodynamic modeling calculated by HSC, temperature is an important factor affecting the decomposition of Al and Fe sulfates. The decomposition of a single sulfate of Al, Fe starts at 300 °C and ends at approximately 800 °C, whereas the decomposition of the composite sulfate of Al, K, and Rb starts at 650 °C and ends at approximately 1000 °C. To selectively recover Li, Rb, and Cs without leaching Al or Fe, the complete decomposition of Al and Fe sulfates is essential. Fig. 6(a) depicts the effect of roasting temperature on the decomposition and

extraction rates of each component in lepidolite ores during roasting S2. The finding disclosed that the extraction of Li, Rb, and Cs was almost unaffected. However, the extraction rates of Al and Fe decreased from 60.3% and 52.6% in the first-step to 38.0% and 8.1% at 700 °C, respectively. This result corresponded to the decomposition of Al$_2$(SO$_4$)$_3$, FeSO$_4$, and Fe$_2$(SO$_4$)$_3$ in the thermodynamic modeling. When the temperature reached 800 °C, the extraction rates declined to 1.20% and 0.51%. As the temperature continued to rise above 850 °C, the extraction rates of Al and Fe were lower than 0.1%, indicating that they were hardly leached at this time. At the same time, the decomposition process produced a large amount of SO$_x$ gas, which could be used for acid production. Calculating based on the concentration of sulfate in the leaching liquor, nearly 90% of sulfur entered the mixed gas. Therefore, most sulfuric acid used in roasting S1 could be recycled through the process of catalytic conversion.

Fig. 7 shows the XRD patterns of roasting slags and leaching residues during roasting S2. The phases of Fe, Rb, and Cs could not be reflected, possibly due to their lower contents and weaker peak intensity, which were covered by the main peaks of K and Al phases. The composition of roasting slags at 700 °C was mainly KAl(SO$_4$)$_2$ and Al$_2$(SO$_4$)$_3$ associated with a small amount of SiO$_2$, which was similar to that after roasting S1. Then, the diffraction peaks of Al$_2$(SO$_4$)$_3$ almost disappeared completely, whereas the peaks of KAl(SO$_4$)$_2$ decreased slightly at 750 °C. Meanwhile, the peaks of KLiSO$_4$ and mullite (Al$_6$Si$_2$O$_{13}$) with relatively weak intensity were formed. When the temperature reached 800 °C, the peaks of KAl(SO$_4$)$_2$ were obliterated entirely as well, and the peaks of KLiSO$_4$ and mullite gradually strengthened. The finding indicated that 800 °C was the demarcation point for the complete decomposition of Al and Fe sulfates, and all of them were converted into insoluble Al and Fe oxides after 800 °C roasting. Fig. 7(b) shows that the leaching residues were
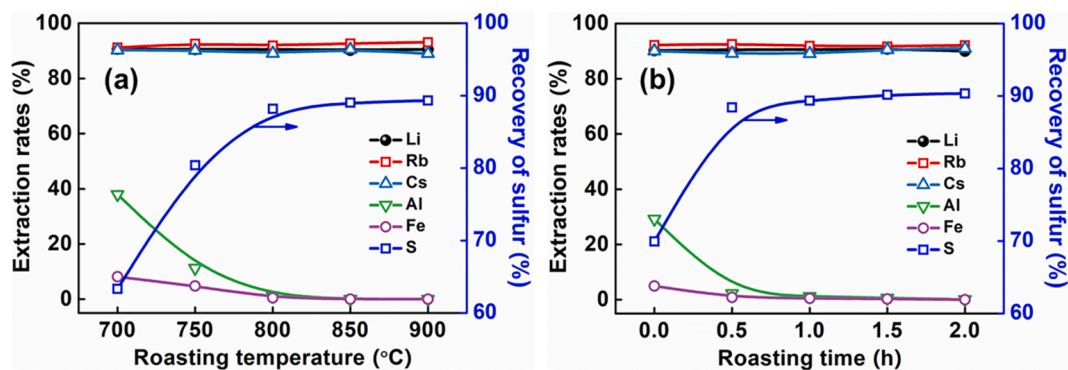
Fig. 6. Effect of (a) roasting temperature (roasting time, 1 h) and (b) roasting time (roasting temperature, 800 °C) on the extraction rates of Li, Rb, Cs, Al, Fe, and the recovery of sulfur during roasting S2.
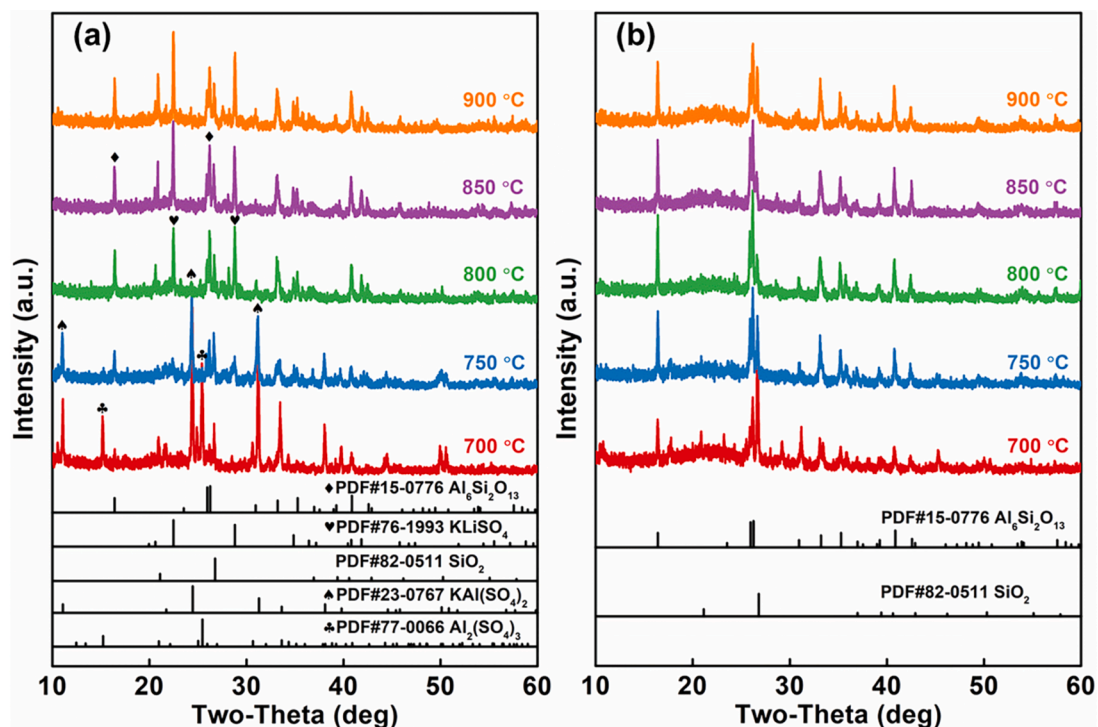
Fig. 7. Effect of roasting temperature on the XRD patterns of (a) roasting slags and (b) leaching residues during roasting S2.

mainly composed of mullite and SiO_2, as well as some Al_2O_3 and Fe_2O_3 not observed in the figure. The undecomposed $KAl(SO_4)_2$, $Al_2(SO_4)_3$, and newly formed $KLiSO_4$ were leached into the liquor. Considering that the phase changes of Rb and Cs were similar to that of K, and that the changes of Fe were similar to Al, the temperature above 800 °C during roasting S2 realized the selective recovery of Li, Rb, and Cs without leaching Al or Fe.

3.3.2. Effect of roasting time

The effect of roasting time on the extraction rates of each component and the recovery of sulfur were discussed, as shown in Fig. 6**(b)**. The temperature remained constant at 800 °C. It indicated that the overall trend of each element was similar to that of temperature, but the change range was relatively small. As the roasting time rose to 0.5 h, the

extraction of Al and Fe decreased rapidly from 29.2% and 5.0% to 2.3% and 0.8%, respectively. Subsequently, the decline slowed considerably, lower than 0.1% until the roasting time reached 2 h. The recovery of sulfur also increased from 69.9% to 88.4% and then tardily to 90.4%. The results indicate that roasting at 800 °C for 2 h was indispensable to achieve the effect of non-leaching of aluminum and iron. The extraction rates of lithium, rubidium and cesium were 90.5%, 91.2%, and 89.4%, respectively, whereas those of aluminum and iron were only 0.08% and 0.02%, respectively. In our proposed new process, the leaching rate of lithium is approximately 90%, which might be affected by two factors. On the one hand, the partly sintering of some minerals might increase the difficulty of water leaching [40]. On the other hand, it might be caused by the slight volatilization of lithium sulfate as well [41].
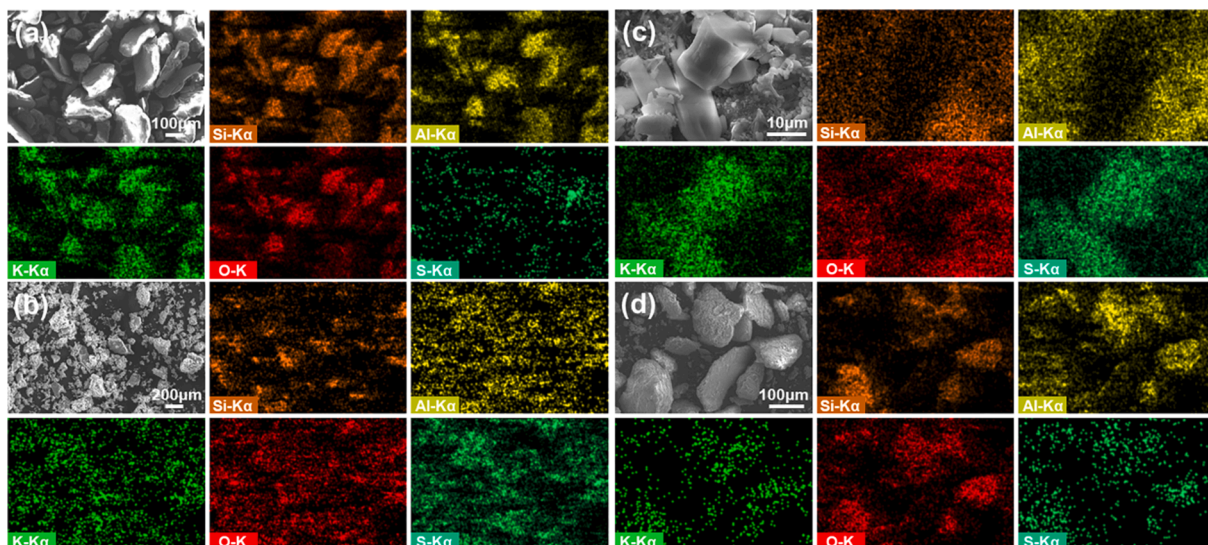
Fig. 8. SEM and EDS mapping for (a) lepidolite ores and solid products after the process of (b) roasting S1, (c) roasting S2, and (d) water leaching.

3.4. Roasting mechanism analysis

Fig. 8 shows the morphology and elemental distribution of the lepidolite ores and the solid phase at each stage of the process. As shown in Fig. 8(a), the lepidolite ores existed in the form of flakes, in which various elements, such as potassium, aluminum, silicon, and oxygen, were distributed uniformly. It contained almost no sulfur component. The SEM-EDS mapping (Fig. 8(b)) indicated that the microstructure had transformed from the overall flake structures to partially irregular particles after roasting S1. The distribution of elements shows that potassium, aluminum, and oxygen still existed widely. Silicon was evidently present only in few flake structures and was hardly present in the newly formed irregular particles. Meanwhile, a large amount of sulfur also entered the slags and was distributed evenly due to the introduction of sulfuric acid. Combined with the XRD analysis of the roasting slags in Fig. 5(b), the irregular particles were mainly $KAl(SO_4)_2$ and $Al_2(SO_4)_3$. Therefore, roasting S1 was the sulfation reaction of lepidolite ores under the interaction with sulfuric acid. The structure of the mineral was destroyed, and the valuable ions were combined with sulfate to form the corresponding sulfate. Fig. 8(c) shows that some angular columnar grains clearly appeared in the solid products after roasting S2. Therefore, the columnar grains were K_2SO_4, ascribed to the distribution in the mapping pattern of potassium, sulfur, and oxygen. In addition, other particles were mainly composed of aluminum, silicon, and oxygen, indicating that the potassium and sulfur in $KAl(SO_4)_2$ and $Al_2(SO_4)_3$ were separated from aluminum. Therefore, roasting S2 was the decomposition reaction of sulfates, in which the soluble aluminum in sulfates was transformed into insoluble aluminum oxides. Combined with the XRD analysis of Fig. 7(b), the aluminum oxides obtained by decomposition and the silicon oxides generated by sulfation formed mullite ($Al_6Si_2O_{13}$), which was more stable. The morphology and elemental distribution of residues after direct leaching with deionized water are shown in Fig. 8(d). The morphology of leaching residues was similar to that of lepidolite ores, which were almost flakes. The aluminum, silicon, and oxygen were evenly distributed, whereas potassium and sulfur were almost absent. This finding indicated that the simple soluble sulfate represented by K_2SO_4 was dissolved into the leaching liquor during the leaching process, and the stable oxides of aluminum and silicon remained in the residues. Therefore, the roasting mechanism was the sulfation of lepidolite ores in the first-step and the decomposition of complex sulfates in the second-step. The separation of alkalis represented by potassium and impurity elements represented by aluminum could be realized by simply deionized water leaching.

3.5. Solvent extraction of rubidium and cesium

The leaching liquor containing 4.15 g/L Li, 13.8 g/L K, 6.21 g/L Rb, and 0.44 g/L Cs was obtained after two-step roasting and water leaching. The rubidium and cesium were selectively solvent extracted with t-BAMBP. The effect of the initial NaOH concentration on the solvent extraction of K, Rb, Cs, and the separation factors ($\beta_{Cs/Rb}$, $\beta_{Rb/K}$) were investigated (1 mol/L t-BAMBP, O/A = 1). As shown in Fig. 9, the solvent extraction of Cs reached more than 80% and that of Rb was approximately 20% when the initial NaOH concentration was 0.2 mol/L. However, only 5 % K was extracted. The solvent extraction of the three elements was positively influenced by the NaOH concentration. According to the variation trend of separation factors, $\beta_{Cs/Rb}$ continued to decrease, indicating that a higher concentration of NaOH was not conducive to the separation of cesium and rubidium. On the contrary, $\beta_{Rb/K}$ presented a trend of increasing initially and then decreasing, reaching the maximum when the NaOH concentration was 0.6 mol/L, depicting the most effective separation.

3.5.1. Separation of rubidium and cesium

Combined with the results, the initial NaOH concentration of the leaching liquor was regulated to 0.2 mol/L, and then solvent extraction of cesium was carried out. Fig. 10(a) shows the effect of t-BAMBP concentration on the solvent extraction of rubidium and cesium (O/A = 1) that of Cs greatly increased from 2.2% to 80.4% as the concentration of t-BAMBP increased from 0.2 to 0.8 mol/L. During this process, the solvent extraction of Rb increased slightly but remained lower than 20%. $\beta_{Cs/Rb}$ showed a trend of rising first and then falling. When the concentration of t-BAMBP was 0.6 mol/L, it reached a maximum value of 31.6, indicating that the separation of cesium and rubidium was the most efficient. However, the solvent extraction of Cs was only approximately 60% at this time; it was lower for a single-stage extraction. The t-BAMBP concentration of 0.8 mol/L was selected for subsequent experiments. Under such conditions, 80.4% Cs was extracted directly, and the separation factor $\beta_{Cs/Rb}$ was 28.8. The effect of the phase ratio (Fig. 10(b)) shows that $\beta_{Cs/Rb}$ was the largest when the O/A was 0.5. Herein, the phase ratio of 1, when $\beta_{Cs/Rb}$ was the second largest, was selected due to the much higher solvent extraction of Cs. Fig. 10(c) depicts the solvent extraction isotherm and McCabe-Thiele diagram of cesium. The diagram shows that when the O/A was selected as 1, Cs in raffinate could be as low as 0.003 g/L after four-stage solvent extraction, and the solvent extraction was 99.3%.

3.5.2. Separation of potassium and rubidium

The separation of potassium and rubidium was studied when the concentration of NaOH was adjusted to 0.6 mol/L. Fig. 11(a, b) discloses the effect of the t-BAMBP concentration (O/A = 1) and phase ratio (1.5 mol/L t-BAMBP). It indicated that the solvent extraction of potassium and rubidium was positively affected. The separation factor ($\beta_{Rb/K}$) initially decreased and then increased with the concentration of t-BAMBP, but it showed a completely opposite change with the phase ratio (initial increase and then decrease). The maximum $\beta_{Rb/K}$ (16.5)
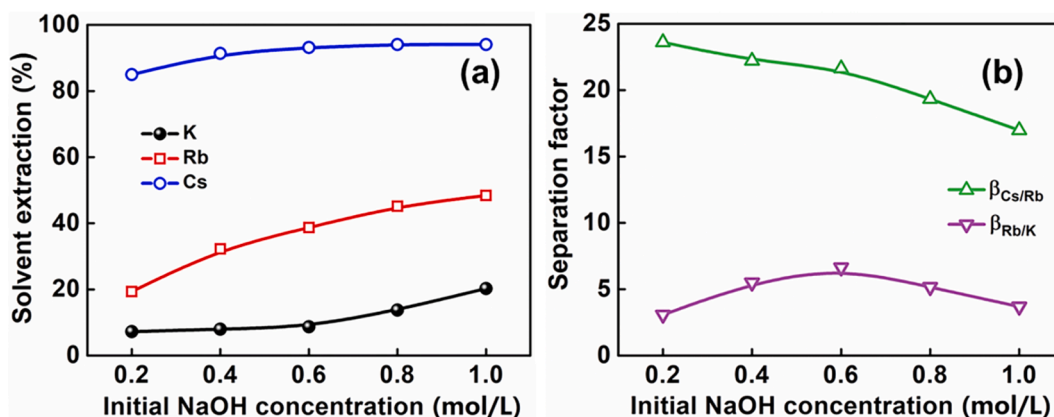
Fig. 9. Effect of initial NaOH concentration on the (a) solvent extraction of K, Rb, Cs, and (b) separation factor of Cs/Rb, Rb/K.
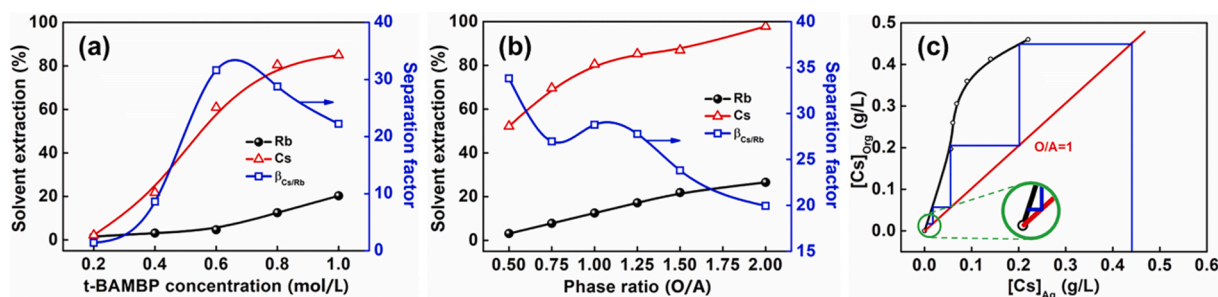
Fig. 10. Effect of (a) t-BAMBP concentration, and (b) phase ratio on the separation of Rb and Cs. (c) Solvent extraction isotherm and McCabe-Thiele diagram of Cs.
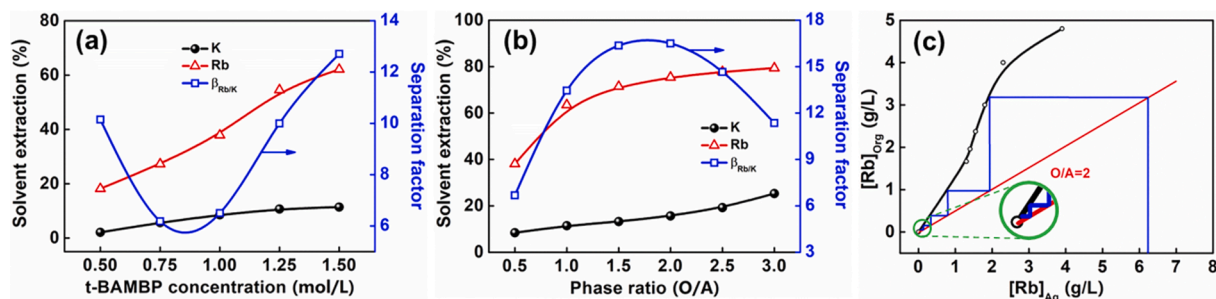
Fig. 11. Effect of (a) t-BAMBP concentration, and (b) phase ratio on the separation of K and Rb. (c) Solvent extraction isotherm and McCabe-Thiele diagram of Rb.

was obtained under the conditions of 1.5 mol/L t-BAMBP and O/A = 2. The solvent extraction isotherm and McCabe-Thiele diagram of rubidium (Fig. 11(c)) showed that when O/A = 2, the concentration of rubidium in raffinate could be as low as 0.047 g/L after five-stage extraction, and the solvent extraction was up to 99.2%.

In summary, solvent extraction realized the selective extraction of cesium and rubidium in leaching liquor. The purified products of cesium and rubidium could be obtained after scrubbing and stripping [42,43]. The feasibility has been verified, and further systematic research would be performed subsequently.

3.6. Precipitation of lithium

The precipitation experiment of lithium was carried out in raffinate containing 4.03 g/L Li, 12.4 g/L Na, and 11.0 g/L K. The traditional precipitant Na_2CO_3 was not used due to the introduction of more Na^+ impurities. CO_2 was selected instead, and the chemical reaction of lithium in this process is shown in **Eqs. (12 and 13)**. Then, $LiHCO_3$ was pyrolyzed (**Eq. (14)**) into Li_2CO_3 during evaporation. At the same time, Li_2CO_3 gradually crystallized due to the decrease in solution volume and the solubility of Li_2CO_3 as the temperature increased. The precipitation rate of lithium increased as the evaporation rate of the solution rose (Fig. 12(a)). However, the content of the main impurities (Na, K) in the

precipitates increased significantly as well. Comprehensively, the evaporation rate was selected as 70%, and the precipitation rate of lithium was 94.1%. The precipitates obtained satisfied the national standard for lithium carbonate (GB/T 11075–2013). The XRD and SEM analysis of the precipitates (Fig. 12(b, c)) demonstrated that they were columnar Li_2CO_3. The pressure of CO_2 is generally approximately 0.4 Mpa, which ensures that the CO_2 in the solution is sufficient to fully react with Li_2CO_3. Industrial production data show that the utilization rate of CO_2 is approximately 75%.

$$2LiOH(l) + CO_2(g) \rightarrow Li_2CO_3(s) + H_2O(l) \tag{12}$$

$$Li_2CO_3(s) + CO_2(g) + H_2O(l) \rightarrow 2LiHCO_3(l) \tag{13}$$

$$2LiHCO_3(l) \rightarrow Li_2CO_3(s) + CO_2(g) + H_2O(l) \tag{14}$$
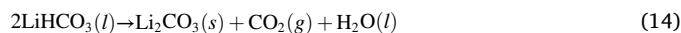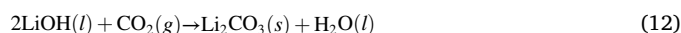
3.7. Proposed process

Based on the results, a schematic of the phase transformation mechanism during the entire process is depicted in Fig. 13. Roasting S1 was the sulfation process of lepidolite. The structure of mineral was destroyed by sulfuric acid, and Li_2SO_4, $Al_2(SO_4)_3$, $(K,Rb,Cs)Al(SO_4)_2$, and SiO_2 were generated. Roasting S2 was the decomposition process of partial sulfates. The single-alkali sulfates obtained were combined with
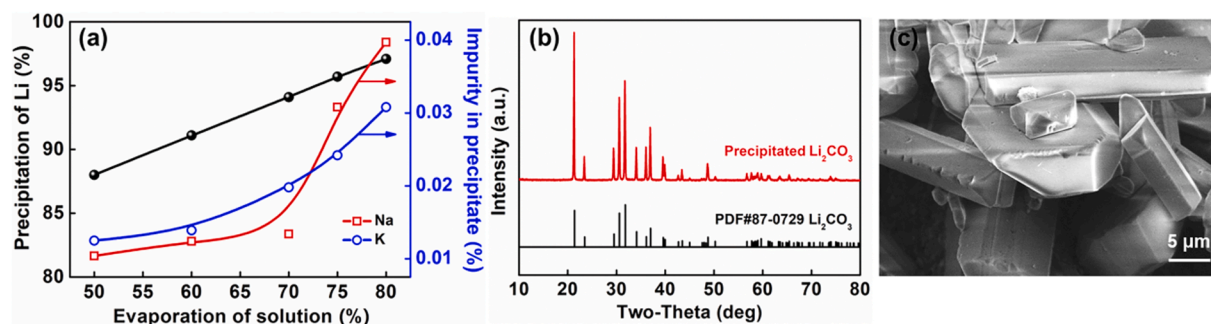
Fig. 12. (a) Effect of the evaporation of solution on the precipitation of lithium; (b) XRD pattern and (c) SEM image of the precipitate when the evaporation was 70%.
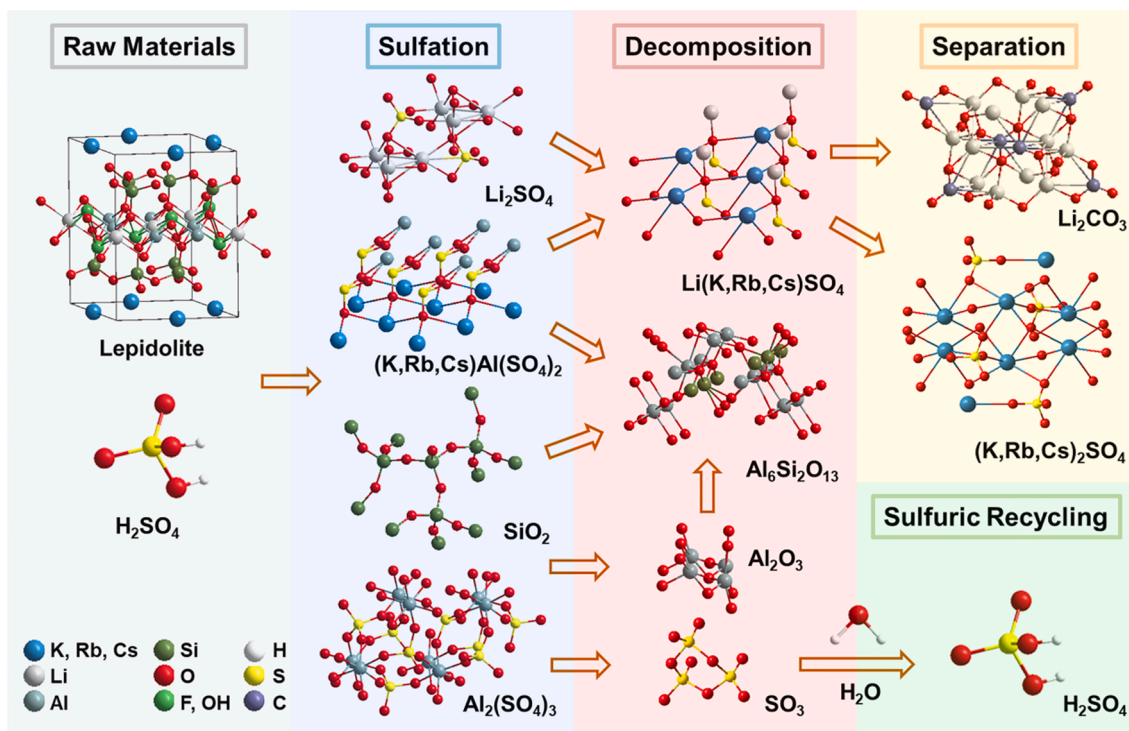
Fig. 13. Schematic of the phase transformation mechanism during the whole process.

Li_2SO_4 to constitute the composite sulfate ($Li(K,Rb,Cs)SO_4$). The Al_2O_3 obtained by decomposition and SiO_2 generated by sulfation formed mullite ($Al_6Si_2O_{13}$). Then, the sulfates in roasting residues were dissolved into aqueous solution during the leaching process. The Li_2CO_3 and single alkali sulfates (K_2SO_4, Rb_2SO_4, and Cs_2SO_4) were produced through the efficient separation methods of carbonization precipitation and solvent extraction. The SO_3 generated during the decomposition process could be used to regenerate sulfuric acid through a mature acid-making process to realize the sulfuric recycling. When treating lepidolite ores with sulfuric acid method, the pH value of leaching solution was usually lower than 1 [34], which indicated the presence of considerable residual acid. A large amount of alkali (CaO or NaOH) was required in the subsequent process to neutralize the residual acid and remove the impurities of iron and aluminum. Our process realized the recycling of sulfuric acid through S2 roasting and avoided residual acid from entering the leaching solution. At the same time, the selective extraction of lithium, rubidium, and cesium from lepidolite ores was achieved, which avoided the alkali consumption in impurity removal as well. The main components of residues were Si, Al, and Fe, which could be used as raw materials in the field of building materials. The solution after lithium precipitation could be returned to the leaching process for recycling. This process achieved the selective recovery and efficient separation of lithium, rubidium, and cesium from lepidolite ores. At the same time, the recycling of sulfuric acid was realized and the amount of reagents such as acid and alkali was greatly reduced. Compared with existing studies, it is an efficient, clean, and sustainable process for the utilization of lepidolite ores.

4. Conclusions

The process was proposed to selectively recover and efficiently separate lithium, rubidium, and cesium from lepidolite ores. The main conclusions are as follows:

(1) Thermodynamic modeling of the process was calculated by HSC Chemistry 6.0 and the theoretical feasibility was verified. The decomposition of $Al_2(SO_4)_3$, $Fe_2(SO_4)_3$, and alum occurred at temperatures of approximately 400 °C, 620 °C, and 650 °C, respectively. The final products were soluble Li_2SO_4, K_2SO_4, and Rb_2SO_4 in water and insoluble Al_2O_3, Fe_2O_3, and gases SO_x.

(2) The optimal parameters were determined as the first-step roasting of 5 h, and the second-step roasting of 800 °C and 2 h. The extraction rates of lithium, rubidium, and cesium were 90.5%, 91.2%, and 89.4%, whereas those of aluminum and iron were only 0.08% and 0.02%, respectively. Selective extraction of lithium, rubidium, and cesium was realized. At the same time, 90.4% sulfuric acid could be recycled, and the amount of reagents, such as acid and alkali, was greatly reduced.

(3) The mechanism was discussed by XRD and SEM-EDS analysis. The results showed that the first-step roasting was the sulfation process of lepidolite ores. The structure of the mineral was destroyed, and the valuable ions were combined with sulfate to form the corresponding sulfate. The second-step roasting was the decomposition process of partial sulfates. The soluble aluminum and iron in sulfates were transformed into insoluble oxides. The separation of alkali elements and impurity elements could be realized by simple leaching.

(4) Rubidium and cesium were selectively solvent extracted by t-BAMBP. The solvent extraction of Cs was 99.3% after four-stage solvent extraction under the conditions of 0.2 mol/L NaOH, 0.8 mol/L t-BAMBP, and O/A = 1. The solvent extraction of Rb was 99.2% after five-stage solvent extraction under the conditions of 0.6 mol/L NaOH, 1.5 mol/L t-BAMBP, and O/A = 2. Columnar Li_2CO_3 that satisfied the national standard (GB/T 11075–2013) was obtained after carbonization precipitation and evaporation; the precipitation rate of lithium reached 94.1%.

This process achieved the selective recovery and efficient separation of lithium, rubidium, and cesium from lepidolite ores. The difficulty of separating lithium and aluminum in the sulfuric acid method was solved. At the same time, the recycling of sulfuric acid was realized, greatly reducing the amount of reagents, such as acid and alkali. It is an efficient, clean, and sustainable process for the utilization of lepidolite ores.

CRediT authorship contribution statement

Yubo Liu: Conceptualization, Writing – original draft, Writing – review & editing. **Baozhong Ma:** Writing – review & editing, Supervision, Project administration. **Yingwei Lv:** Resources, Validation. **Chengyan Wang:** Supervision, Project administration, Funding acquisition. **Yongqiang Chen:** Validation, Visualization.

Declaration of Competing Interest

The authors declare that they have no known competing financial interests or personal relationships that could have appeared to influence the work reported in this paper.

Acknowledgements

References

[1] J.-M. Tarascon, M. Armand, Issues and challenges facing rechargeable lithium batteries, Nature 414 (6861) (2001) 359–367, https://doi.org/10.1038/35104644.

[2] J. Hou, H. Zhang, A.W. Thornton, A.J. Hill, H. Wang, K. Konstas, Lithium extraction by emerging metal-organic framework-based membranes, Adv. Funct. Mater. 31 (2021) 2105991, https://doi.org/10.1002/adfm.202105991.

[3] C. Helbig, A.M. Bradshaw, L. Wietschel, A. Thorenz, A. Tuma, Supply risks associated with lithium-ion battery materials, J. Clean. Prod. 172 (2018) 274–286, https://doi.org/10.1016/j.jclepro.2017.10.122.

[4] P. Xing, C. Wang, L. Zeng, B. Ma, L. Wang, Y. Chen, C. Yang, Lithium extraction and hydroxysodalite zeolite synthesis by hydrothermal conversion of α-spodumene, ACS Sustain. Chem. Eng. 7 (2019) 9498–9505. http://doi.org/10.1021/acssuschemeng.9b00923.

[5] U.S. Geological Survey, Mineral commodity summaries 2011. U.S. Geological Survey, 2011. 10.3133/mineral2011.

[6] U.S. Geological Survey. Mineral commodity summaries 2021. U.S. Geological Survey, 2021. 10.3133/mcs2021.

[7] C. Chaves, E. Pereira, P. Ferreira, A. Guerner Dias, Concerns about lithium extraction: A review and application for Portugal, Extr. Ind. Soc. 8 (2021) 100928, https://doi.org/10.1016/j.exis.2021.100928.

[8] B. Scrosati, J. Garche, Lithium batteries: Status, prospects and future, J. Power Sources 195 (9) (2010) 2419–2430, https://doi.org/10.1016/j.jpowsour.2009.11.048.

[9] S. Ferrari, M. Falco, A.B. Munoz-Garcia, M. Bonomo, S. Brutti, M. Pavone, C. Gerbaldi, Solid-state post Li metal ion batteries: A sustainable forthcoming reality? Adv. Energy Mater. 11 (2021) 2100785, https://doi.org/10.1002/aenm.202100785.

[10] G. Naidu, T. Nur, P. Loganathan, J. Kandasamy, S. Vigneswaran, Selective sorption of rubidium by potassium cobalt hexacyanoferrate, Sep. Purif. Technol. 163 (2016) 238–246, https://doi.org/10.1016/j.seppur.2016.03.001.

[11] M. Saliba, T. Matsui, K. Domanski, J.-Y. Seo, A. Ummadisingu, S.M. Zakeeruddin, J.-P. Correa-Baena, W.R. Tress, A. Abate, A. Hagfeldt, M. Grätzel, Incorporation of rubidium cations into perovskite solar cells improves photovoltaic performance, Science 354 (6309) (2016) 206–209.

[12] P. Xing, C. Wang, Y. Chen, B. Ma, Rubidium extraction from mineral and brine resources: A review, Hydrometallurgy 203 (2021) 105644, https://doi.org/10.1016/j.hydromet.2021.105644.

[13] G. Naidu, S. Jeong, M.A.H. Johir, A.G. Fane, J. Kandasamy, S. Vigneswaran, Rubidium extraction from seawater brine by an integrated membrane distillation-selective sorption system, Water Res. 123 (2017) 321–331, https://doi.org/10.1016/j.watres.2017.06.078.

[14] Q. Bouton, J. Nettersheim, S. Burgardt, D. Adam, E. Lutz, A. Widera, A quantum heat engine driven by atomic collisions, Nat. Commun. 12 (2021) 2063, https://doi.org/10.1038/s41467-021-22222-z.

[15] T. Nur, P. Loganathan, M.A.H. Johir, J. Kandasamy, S. Vigneswaran, Removing rubidium using potassium cobalt hexacyanoferrate in the membrane adsorption hybrid system, Sep. Purif. Technol. 191 (2018) 286–294, https://doi.org/10.1016/j.seppur.2017.09.048.

[16] J. Tian, L. Xu, H. Wu, S. Fang, W. Deng, T. Peng, W. Sun, Y. Hu, A novel approach for flotation recovery of spodumene, mica and feldspar from a lithium pegmatite ore, J. Clean. Prod. 174 (2018) 625–633, https://doi.org/10.1016/j.jclepro.2017.10.331.

[17] L.P. Ogorodova, I.A. Kiseleva, L.V. Melchakova, T.N. Schuriga, Thermodynamic properties of lithium mica: Lepidolite, Thermochim. Acta 435 (1) (2005) 68–70, https://doi.org/10.1016/j.tca.2005.04.026.

[18] S.E. Kesler, P.W. Gruber, P.A. Medina, G.A. Keoleian, M.P. Everson, T. J. Wallington, Global lithium resources: Relative importance of pegmatite, brine and other deposits, Ore Geol. Rev. 48 (2012) 55–69, https://doi.org/10.1016/j.oregeorev.2012.05.006.

[19] B. Tadesse, F. Makuei, B. Albijanic, L. Dyer, The beneficiation of lithium minerals from hard rock ores: A review, Miner. Eng. 131 (2019) 170–184, https://doi.org/10.1016/j.mineng.2018.11.023.

[20] H. Li, G.e. Kuang, S. Hu, H. Guo, R. Jin, R.L. Vekariya, Removal of aluminum from leaching solution of lepidolite by adding ammonium, JOM 68 (10) (2016) 2653–2658, https://doi.org/10.1007/s11837-016-2080-1.

[21] Q. Zeng, S. Li, W. Sun, L. Hu, H. Zhong, Z. He, Eco-friendly leaching of rubidium from biotite-containing minerals with oxalic acid and effective removal of Hg^{2+} from aqueous solution using the leaching residues, J. Clean. Prod. 306 (2021) 127167, https://doi.org/10.1016/j.jclepro.2021.127167.

[22] H. Su, J. Ju, J. Zhang, A. Yi, Z. Lei, L. Wang, Z. Zhu, T. Qi, Lithium recovery from lepidolite roasted with potassium compounds, Miner. Eng. 145 (2020), 106087, https://doi.org/10.1016/j.mineng.2019.106087.

[23] N. Vieceli, C.A. Nogueira, M.F.C. Pereira, F.O. Durão, C. Guimarães, F. Margarido, Optimization of lithium extraction from lepidolite by roasting using sodium and calcium sulfates, Miner. Process. Extr. Metall. Rev. 38 (1) (2017) 62–72, https://doi.org/10.1080/08827508.2016.1262858.

[24] T. Ncube, H. Oskierski, G. Senanayake, B.Z. Dlugogorski, Two-step reaction mechanism of roasting spodumene with potassium sulfate, Inorg. Chem. 60 (2021) 3620–3625. http://doi.org/10.1021/acs.inorgchem.0c03125.

[25] Q.-X. Yan, X.-H. Li, Z.-X. Wang, J.-x. Wang, H.-J. Guo, Q.-Y. Hu, W.-J. Peng, X.-F. Wu, Extraction of lithium from lepidolite using chlorination roasting-water leaching process, Trans. Nonferrous Met. Soc. China 22 (7) (2012) 1753–1759.

[26] B. Swain, Recovery and recycling of lithium: A review, Sep. Purif. Technol. 172 (2017) 388–403, https://doi.org/10.1016/j.seppur.2016.08.031.

[27] X. Zhang, T. Aldahri, X. Tan, W. Liu, L. Zhang, S. Tang, Efficient co-extraction of lithium, rubidium, cesium and potassium from lepidolite by process intensification of chlorination roasting, Chem. Eng. Process. Process Intensif. 147 (2020) 10777, https://doi.org/10.1016/j.cep.2019.107777.

[28] Y. Liu, B. Ma, Y. Lv, C. Wang, Y. Chen, Thorough extraction of lithium and rubidium from lepidolite via thermal activation and acid leaching, Miner. Eng. 178 (2022), https://doi.org/10.1016/j.mineng.2022.107407.

[29] H. Guo, M. Lv, G. Kuang, Y. Cao, H. Wang, Stepwise heat treatment for fluorine removal on selective leachability of Li from lepidolite using HF/H_2SO_4 as lixiviant, Sep. Purif. Technol. 259 (2021), 118194, https://doi.org/10.1016/j.seppur.2020.118194.

[30] G.D. Rosales, E.G. Pinna, D.S. Suarez, M.H. Rodriguez, Recovery process of Li, Al and Si from lepidolite by leaching with HF, Minerals 7 (2017) 36, https://doi.org/10.3390/min7030036.

[31] H.-D. Wang, A.-a. Zhou, H. Guo, M.-H. Lü, H.-Z. Yu, Kinetics of leaching lithium from lepidolite using mixture of hydrofluoric and sulfuric acid, J. Cent. South Univ. 27 (1) (2020) 27–36, https://doi.org/10.1007/s11771-020-4275-4.

[32] J. Mulwanda, G. Senanayake, H. Oskierski, M. Altarawneh, B.Z. Dlugogorski, Leaching of lepidolite and recovery of lithium hydroxide from purified alkaline pressure leach liquor by phosphate precipitation and lime addition, Hydrometallurgy 201 (2021) 105538, https://doi.org/10.1016/j.hydromet.2020.105538.

[33] Y. Lv, P. Xing, B. Ma, Y. Liu, C. Wang, W. Zhang, Y. Chen, Efficient extraction of lithium and rubidium from polylithionite via alkaline leaching combined with solvent extraction and precipitation, ACS Sustain. Chem. Eng. 8 (38) (2020) 14462–14470, https://doi.org/10.1021/acssuschemeng.0c04437.

[34] N. Vieceli, C.A. Nogueira, M.F.C. Pereira, F.O. Durao, C. Guimaraes, F. Margarido, Recovery of lithium carbonate by acid digestion and hydrornetallurgical processing from mechanically activated lepidolite, Hydrometallurgy 175 (2018) 1–10, https://doi.org/10.1016/j.hydromet.2017.10.022.

[35] N. Vieceli, C.A. Nogueira, M.F.C. Pereira, F.O. Durão, C. Guimarães, F. Margarido, Optimization of an innovative approach involving mechanical activation and acid digestion for the extraction of lithium from lepidolite, Int. J. Miner. Metall. Mater. 25 (1) (2018) 11–19, https://doi.org/10.1007/s12613-018-1541-7.

[36] J. Liu, Z. Yin, X. Li, Q. Hu, W. Liu, A novel process for the selective precipitation of valuable metals from lepidolite, Miner. Eng. 135 (2019) 29–36, https://doi.org/10.1016/j.mineng.2018.11.046.

[37] X. Zhang, X. Tan, C. Li, Y. Yi, W. Liu, L. Zhang, Energy-efficient and simultaneous extraction of lithium, rubidium and cesium from lepidolite concentrate via sulfuric acid baking and water leaching, Hydrometallurgy 185 (2019) 244–249, https://doi.org/10.1016/j.hydromet.2019.02.011.

[38] J.B. Champenois, A. Mesbah, A. Dannoux-Papin, C. Cau Dit Coumes, N. Dacheux, $LiAl(OH)_6OH \cdot 2H_2O$ solubility product and dihydrogen radiolytic production rate under γ-irradiation, J. Nucl. Mater. 508 (2018) 92–99, https://doi.org/10.1016/j.jnucmat.2018.05.013.

[39] S. Britto, P.V. Kamath, Polytypism in the lithium-aluminum layered double hydroxides: the $[LiAl_2(OH)_6]^+$ layer as a structural synthon, Inorg. Chem. 50 (2011) 5619–5627, https://doi.org/10.1021/ic200312g.

[40] P. Xing, C. Wang, B. Ma, L. Wang, W. Zhang, Y. Chen, Rubidium and potassium extraction from granitic rubidium ore: Process optimization and mechanism study, ACS Sustain. Chem. Eng. 6 (2018) 4922–4930. http://doi.org/10.1021/acssuschemeng.7b04445.

[41] D. Yelatontsev, A. Mukhachev, Processing of lithium ores: Industrial technologies and case studies - A review, Hydrometallurgy 201 (2021), https://doi.org/10.1016/j.hydromet.2021.105578.

[42] D. Pang, Z. Zhang, Y. Zhou, Z. Fu, Q. Li, Y. Zhang, G. Wang, Z. Jing, The process and mechanism for cesium and rubidium extraction with saponified 4-tert-butyl-2-(α-methylbenzyl) phenol, Chin. J. Chem. Eng. (2021), https://doi.org/10.1016/j.cjche.2021.07.001.

[43] P. Xing, G. Wang, C. Wang, B. Ma, Y. Chen, Separation of rubidium from potassium in rubidium ore liquor by solvent extraction with t-BAMBP, Miner. Eng. 121 (2018) 158–163, https://doi.org/10.1016/j.mineng.2018.03.014.